

Aperture-averaged scintillation index and fade statistics in weak oceanic turbulence

Hao Wang(王昊), Fu-Zeng Kang(康福增), Xuan Wang(王瑄), Wei Zhao(赵卫), and Shu-Wei Sun(孙枢为)
Citation: Chin. Phys. B, 2021, 30 (**6**): 064207. DOI: 10.1088/1674-1056/abd756
Journal homepage: http://cpb.iphy.ac.cn; http://iopscience.iop.org/cpb

What follows is a list of articles you may be interested in

Multiple scattering and modeling of laser in fog

Ji-Yu Xue(薛积禹), Yun-Hua Cao(曹运华), Zhen-Sen Wu(吴振森), Jie Chen(陈杰), Yan-Hui Li(李艳辉), Geng Zhang(张耿), Kai Yang(杨凯), and Ruo-Ting Gao(高若婷)
Chin. Phys. B, 2021, 30 (**6**): 064206. DOI: 10.1088/1674-1056/abddab

Properties of off-axis hollow Gaussian-Schell model vortex beam propagating in turbulent atmosphere

Yan-Song Song(宋延嵩), Ke-Yan Dong(董科研), Shuai Chang(常帅), Yan Dong(董岩), Lei Zhang(张雷)
Chin. Phys. B, 2020, 29 (**6**): 064213. DOI: 10.1088/1674-1056/ab836c

A hybrid method of solving near-zone composite eletromagnetic scattering from targets and underlying rough surface

Xi-Min Li(李西敏), Jing-Jing Li(李晶晶), Qian Gao(高乾), Peng-Cheng Gao(高鹏程)
Chin. Phys. B, 2020, 29 (**2**): 024202. DOI: 10.1088/1674-1056/ab5ef9

Properties of multi-Gaussian Schell-model beams carrying an edge dislocation propagating in oceanic turbulence

Da-Jun Liu(刘大军), Yao-Chuan Wang(王耀川), Gui-Qiu Wang(王桂秋), Hong-Ming Yin(尹鸿鸣), Hai-Yang Zhong(仲海洋)
Chin. Phys. B, 2019, 28 (**10**): 104207. DOI: 10.1088/1674-1056/ab3f21

Electromagnetic scattering of charged particles in a strong wind-blown sand electric field

Xingcai Li(李兴财), Xuan Gao(高璇), Juan Wang(王娟)
Chin. Phys. B, 2019, 28 (**3**): 034208. DOI: 10.1088/1674-1056/28/3/034208

Aperture-averaged scintillation index and fade statistics in weak oceanic turbulence*

Hao Wang(王昊)[1,2], Fu-Zeng Kang(康福增)[1,†], Xuan Wang(王瑄)[3,4,‡], Wei Zhao(赵卫)[1], and Shu-Wei Sun(孙枢为)[1,2]

[1] *State Key Laboratory of Transient Optics and Photonics, Xi'an Institute of Optics and Precision Mechanics, Chinese Academy of Sciences, Xi'an* 710119, *China*

[2] *University of Chinese Academy of Sciences, Beijing* 100049, *China*

[3] *Beijing National Laboratory for Condensed Matter Physics, Institute of Physics, Chinese Academy of Sciences, Beijing* 100190, *China*

[4] *Songshan Lake Materials Laboratory, Dongguan* 523808, *China*

(Received 14 October 2020; revised manuscript received 10 December 2020; accepted manuscript online 30 December 2020)

With the rapid demand for underwater optical communication (UOC), studies of UOC degradation by oceanic turbulence have attached increasing attention worldwide and become a research hot-spot in recent years. Previous studies used a simplified and inaccurate oceanic turbulence spectrum, in which the eddy diffusivity ratio between temperature and salinity is assumed to be unity and the outer scale of turbulence is assumed to be infinite. However, both assumptions are not true in most of the actual marine environments. In this paper, based on the Rytov theory in weak turbulence, we derive analytical expressions of "the aperture-averaged scintillation index" (SI) for both plane and spherical waves, which can clearly demonstrate how SI is influenced by several key factors in UOC. Then, typical fade statistics of the UOC system in weak turbulence is discussed including the probability of fade, the expected number of fades per time, the mean fade time, signal-to-noise ratio and bit error rate. Our results show that spherical wave is preferable in the UOC system in weak turbulence compared to plane wave, and the aperture-averaged effect has a significant impact on UOC system's performance. Our results can be used to determine those key parameters for designing the UOC system over reasonable ranges.

Keywords: underwater optical communication (UOC), aperture-averaged scintillation index, fade statistics

PACS: 42.68.Xy, 42.68.Ay, 42.25.Bs **DOI:** 10.1088/1674-1056/abd756

1. Introduction

Underwater optical communication (UOC) has gained increasing attention in recent years for the increasing demand of military applications.[1–3] It has obvious advantage over the underwater acoustic communication in many aspects, etc., large data capacity, and low-time delay in short to medium distance. However, propagation of a laser beam used in UOC is seriously limited by oceanic turbulence, causing the degradation of UOC performance. To tackle this issue, Nikishov and Nikishov firstly proposed an oceanic turbulence spectrum, providing a foundation for further analysis of oceanic turbulence.[4] Since then, there have been some studies on "the aperture-averaged scintillation index" (SI) and performance of UOC in oceanic turbulence based on Nikishov's spectrum. For example, Korotkova presented numerical simulation of SI of both plane and spherical waves in weak oceanic turbulence.[5] Wang *et al.*[6] gave an analytical expression of SI by geometrical optics approximation. Yi *et al.*[7,8] also analyzed SI of both plane and spherical waves in weak oceanic turbulence and showed that using large-aperture receiver can remarkably decrease SI and consequently improve the system performance significantly. Recently, Gokce and Baykal[9,10] systematically studied how the aperture's size of the receiver affects SI in strong oceanic turbulence.

Although much progress has been made in this field, the validity of them in real situation is strongly restricted by Nikishov's spectrum, which is over-simplified in describing turbulence in several aspects. For example, it assumes that seawater has a stable stratification, that is, the larger the density is, the lower it lies, so that the eddy diffusivity ratio is equal to unity. However, because the surface water is affected by winds and heat exchanges with atmosphere, it is usually neither stable nor layered. Especially at medium and high latitude on earth, the density stratification is reduced or even disappeared.[11] Awareness of such a problem in Nikishov's spectrum, Yue *et al.*[12] proposed a modified power spectrum model, which took the instability of stratification into account. Furthermore, their spectrum considered the outer scale of the turbulence as a variable rather than setting it to be infinite. Based on this new model, they investigated how laser beam wanders in weak turbulence. Their results are very different from those using Nikishov's spectrum. They also showed that the wander of a laser beam with Gaussian intensity profile is significantly reduced by decreasing the outer scale of turbulence. It seems promising that Yue's spectrum can bring new insight to the theoretical studies of UOC systems. However, to our knowledge, no such

*Project supported by the fund from Xi'an Institute of Optics and Precision Mechanics.

†Corresponding author. E-mail: kangfuzeng@opt.ac.cn

‡Corresponding author. E-mail: xw@iphy.ac.cn

© 2021 Chinese Physical Society and IOP Publishing Ltd

research of UOC systems by applying Yue's spectrum is available yet.

In this study, we present an improved model of a UOC system in weak oceanic turbulence based on Yue's spectrum.[12] We derive the analytic expressions of SI in weak oceanic turbulence and carry out a numerical simulation. It is found that spherical wave is preferable in the UOC system in weak turbulence compared to plane wave, and the aperture-averaged effect has a significant impact on UOC system's performance. We further discuss some typical fade statistics of the UOC system including the probability of fade, the expected number of fades per time and the mean fade time, signal-to-noise ratio (SNR) and bit error rate (BER), according to the numerical simulation. Particularly, the eddy diffusivity ratio and the outer scale of the turbulence are considered[11] in our model and their effect on SI is discussed.

2. Theory

2.1. The oceanic turbulence power spectrum with the eddy diffusivity ratio and the outer scale

Let us firstly briefly introduce Yue's spectrum used in our model. In 2019, Yue *et al.*[12] presented an oceanic turbulence power spectrum $\Phi_n(\kappa)$, which includes the temperature spectrum $\Phi_{\rm T}(\kappa)$, the salinity spectrum $\Phi_{\rm S}(\kappa)$, and the coupling spectrum $\Phi_{\rm TS}(\kappa)$. The power spectrum of oceanic turbulence is expressed as

$$\Phi_n(\kappa) = \Phi_{\rm T}(\kappa)+\Phi_{\rm S}(\kappa)-\Phi_{\rm TS}(\kappa), \tag{1}$$

$$\Phi_{\rm T}(\kappa) = (4\pi)^{-1}C_0\alpha^2\chi_{\rm T}\varepsilon^{-\frac{1}{3}}\left(\kappa^2+\kappa_0^2\right)^{-\frac{11}{6}} \times\left[1+C_{\rm T}(\kappa\eta)^{\frac{2}{3}}\right]\exp\left[-\frac{(\kappa\eta)^2}{N_{\rm T}^2}\right], \tag{2}$$

$$\Phi_{\rm S}(\kappa) = (4\pi)^{-1}C_0\alpha^2\chi_{\rm T}\varepsilon^{-\frac{1}{3}}\left(\kappa^2+\kappa_0^2\right)^{-\frac{11}{6}}\frac{d_{\rm r}}{w^2} \times\left[1+C_{\rm S}(\kappa\eta)^{\frac{2}{3}}\right]\exp\left[-\frac{(\kappa\eta)^2}{N_{\rm S}^2}\right], \tag{3}$$

$$\Phi_{\rm TS}(\kappa) = (4\pi)^{-1}C_0\alpha^2\chi_{\rm T}\varepsilon^{-\frac{1}{3}}\left(\kappa^2+\kappa_0^2\right)^{-\frac{11}{6}}\frac{1+d_{\rm r}}{w} \times\left[1+C_{\rm TS}(\kappa\eta)^{\frac{2}{3}}\right]\exp\left[-\frac{(\kappa\eta)^2}{N_{\rm TS}^2}\right], \tag{4}$$

where κ is the magnitude of the spatial frequency; α is the thermal expansion coefficient, which is related to the temperature and salinity of the marine environment; $\kappa_{0=}2\pi/L_0$ (L_0 is the outer scale of turbulence); ε is the dissipation rate of turbulent kinetic energy per unit mass of fluid in the range from 10^{-1} m^2/s^3 to 10^{-10} m^2/s^3. C_0 is a constant equal to 0.72. In Eqs. (2)–(4), η is Kolmogorov microscale length (inner scale); $\chi_{\rm T}$ is the dissipation rate of mean-squared temperature, varying from 10^{-4} K^2/s to 10^{-10} K^2/s; w is a dimensionless parameter providing the ratio between temperature and salinity that contributions to the refractive index spectrum ranging from -5 to 0. $P_{\rm T}$, $P_{\rm S}$ and $P_{\rm TS}$ are the Prandtl number of temperature, salinity, and the coupled temperature salinity, respectively, where $P_{\rm TS}=2P_{\rm T}P_{\rm S}/(P_{\rm T}+P_{\rm S})$. C_i ($i=$ T, S or TS) is a constant related to Φ_i. N_i is a function of the Prandtl number P_i, governing the upper bound for the inertial-diffusive range of Φ_i, which can be written as

$$N_i = 3Q^{-3/2}\left(W_i-\frac{1}{3}+\frac{1}{9W_i}\right)^{3/2}, \tag{5}$$

$$W_i = \left\{\left[\left(\frac{1}{27}-\frac{P_iQ^2}{6C_0}\right)^2-\frac{1}{729}\right]^{1/2}-\left(\frac{1}{27}-\frac{P_iQ^2}{6C_0}\right)\right\}^{1/3}. \tag{6}$$

The eddy diffusivity ratio d_r is given by

$$d_{\rm r} = \begin{cases}\sqrt{w(w+1)}-w, & -5\le w\le -1,\\ -(1.85w+0.85), & -1<w<-0.5,\\ -0.15w, & -0.5\le w\le 0.\end{cases} \tag{7}$$

From Eq. (7), it can be seen that $d_{\rm r}$ is a segmented function of w. However, in previous studies using Nikishov's spectrum, $d_{\rm r}$ is treated as unity, independent of w.

2.2. Aperture-averaged SI and fade statistics

SI of plane and spherical waves in weak turbulence is defined as[13]

$$\sigma_{\rm I,pl}^2(L) = 8\pi^2k^2L\int_0^1\int_0^\infty\kappa\Phi_{\rm n}(\kappa)\exp\left(-\frac{D^2\kappa^2}{16}\right) \times\left[1-\cos\left(\frac{L\kappa^2}{k}\xi\right)\right]{\rm d}\kappa{\rm d}\xi, \tag{8}$$

$$\sigma_{\rm I,sp}^2(L) = 8\pi^2k^2L\int_0^1\int_0^\infty\kappa\Phi_{\rm n}(\kappa)\exp\left(-\frac{D^2\kappa^2\xi^2}{16}\right) \times\left\{1-\cos\left[\frac{L\kappa^2}{k}\xi(1-\xi)\right]\right\}{\rm d}\kappa{\rm d}\xi, \tag{9}$$

where $\sigma_{\rm I,pl}^2$ and $\sigma_{\rm I,sp}^2$ represent SI of plane and spherical waves in oceanic turbulence, respectively; k is the wave number given by $k=2\pi/\lambda$ with λ being the wavelength of light; L is the propagation distance; ξ is the normalized path length given by $\xi=1-z/L$; and D is the receive aperture diameter.

Substituting Eq. (1) into Eqs. (8) and (9), SI of plane and spherical waves can be expressed as

$$\sigma_{\rm I,pl}^2 = 2\pi k^2L\alpha^2C_0\chi_{\rm T}\varepsilon^{-1/3} \times\left(I_{\rm T,pl}+\frac{d_{\rm r}}{w^2}I_{\rm S,pl}-\frac{1+d_{\rm r}}{w}I_{\rm TS,pl}\right), \tag{10}$$

$$\sigma_{\rm I,sp}^2 = 2\pi k^2L\alpha^2C_0\chi_{\rm T}\varepsilon^{-1/3} \times\left(I_{\rm T,sp}+\frac{d_{\rm r}}{w^2}I_{\rm S,sp}-\frac{1+d_{\rm r}}{w}I_{\rm TS,sp}\right). \tag{11}$$

We leave the detailed calculation of SI in the Appendix.

Referring to the mathematical model for the probability density function (PDF) of the randomly fading irradiance signal, we discuss the probability of fade, the expected number of fades per time, the mean fade time below a prescribed threshold, SNR and BER.

The probability of fade can be expressed as[13]

$$\Pr_j(I \le I_{\rm T}) = \frac{1}{2}\left\{1+\mathrm{erf}\left[\frac{0.5\sigma_{{\rm I},j}^2 - 0.23F_{\rm T}}{\sqrt{2}\sigma_{{\rm I},j}^2}\right]\right\}, \quad (12)$$

where $j = $ pl or sp represents plane and spherical waves, respectively; $\mathrm{erf}(x)$ is the error function. The fade parameter $F_{\rm T}$, given in decibels (dB), represents the dB level below the on-axis mean irradiance.

The number of negative crossing of a prescribed threshold $\langle n(I_{\rm T})\rangle$ characterizes the expected number of fades per time, which can be expressed as

$$\langle n(I_{\rm T})\rangle_j = \nu_0 \exp\left[-\frac{\left(0.5\sigma_{{\rm I},j}^2 - 0.23F_{\rm T}\right)^2}{2\sigma_{{\rm I},j}^2}\right], \quad (13)$$

where $\langle\cdots\rangle$ represents the ensemble average and ν_0 is the quasi-frequency.

Mean fade time $\langle t(I_{\rm T})\rangle$ can be written as

$$\langle t(I_{\rm T})\rangle_j = \frac{\Pr_j(I \le I_{\rm T})}{\langle n(I_{\rm T})\rangle_j}. \quad (14)$$

For a shot-noise-limited system, the SNR at the output of the detector can be written as[5,7,8]

$$\langle \mathrm{SNR}\rangle_j = \frac{\mathrm{SNR}_0}{\sqrt{1+\sigma_{{\rm I},j}^2 \mathrm{SNR}_0}}, \quad (15)$$

where SNR_0 is the SNR in the absence of turbulence.

In the presence of oceanic turbulence, the probability of error is considered to be a conditional probability that must be averaged over the PDF of the random signal to determine the unconditional mean BER. In terms of a normalized signal with unit mean, it leads to the expression[5,7,8]

$$\langle \mathrm{BER}\rangle_j = \frac{1}{2}\int_0^\infty p_{{\rm I},j}(u)\,\mathrm{erfc}\left(\frac{\langle \mathrm{SNR}\rangle_j u}{2\sqrt{2}}\right)\mathrm{d}u, \quad (16)$$

where $p_{\rm I}(u)$ is taken to be the gamma-gamma distribution[5]

$$p_{{\rm I},j}(u) = \frac{1}{u\sigma_{{\rm I},j}\sqrt{2\pi}}\exp\left\{-\frac{\left[\ln u + 0.5\sigma_{{\rm I},j}^2\right]^2}{2\sigma_{{\rm I},j}^2}\right\}, \quad u>0. \quad (17)$$

3. Result and discussion

In this section, we present some numerical results based on our model. All the expressions developed in the paper are restricted to weak turbulence, so we limit the SI below 1.[7] A typical marine environment is considered, in which the salinity is 35% and temperature is 20 °C,[10] $\alpha = 2.56\times10^{-4}$ L/°C, $P_{\rm T} = 7$, $P_{\rm S} = 700$, $P_{\rm TS} = 13.86$, $C_{\rm T} = 2.18$, $C_{\rm S} = 2.22$ and $C_{\rm TS} = 2.21$,[10] $\chi_{\rm T} = 10^{-7}$ K^2/s, $\varepsilon = 10^{-4}$ m^2/s^3. We set the wavelength $\lambda = 532$ nm in the calculation, which is in the range of light window[14] (470–580 nm) for the seawater.

Notably, although we introduce outer scale L_0 in the analytical expression of SI for both plane and spherical waves in Eqs. (10) and (11), L_0 has negligible effect on SI (details are not shown here) similar to that in atmosphere turbulence. This justifies setting it to be infinite in previous studies.[15]

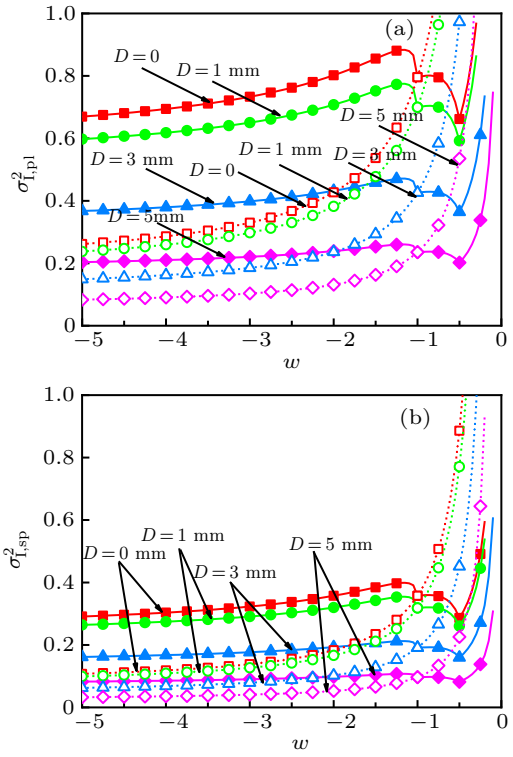


Fig. 1. SI of plane wave (a) and spherical wave (b) versus w for various receive aperture diameters. The solid lines are with $d_{\rm r}$ calculated by Eq. (7), while dotted lines are with $d_{\rm r} = 1$. The red solid/dotted lines represent $D = 0$ mm, the green solid/dotted lines represent $D = 1$ mm, the blue solid/dotted lines represent $D = 3$ mm and the magenta lines represent $D = 5$ mm, respectively. For all the curves, $L = 20$ m and $\eta = 10^{-3}$ m.

Firstly, we study how SI varies according to w, η and L one by one. Figure 1 shows $\sigma_{\rm I,pl}^2$ and $\sigma_{\rm I,sp}^2$ as functions of w for various D in two cases ($d_{\rm r}$ calculated by Eq. (7) and $d_{\rm r} = 1$). $D = 0$ mm corresponds to the point receiver. Since $d_{\rm r}$ is separated into three pieces in Eq. (7), the curves of $\sigma_{\rm I,pl}^2$ and $\sigma_{\rm I,sp}^2$ (solid line) in this case can also be divided into three sections. In the first section, $\sigma_{\rm I,pl}^2$ and $\sigma_{\rm I,sp}^2$ initially increase as w increases, reaching a maximum when w is about 1.15, and then decreases as w approaches -1. However, the overall changes of $\sigma_{\rm I,pl}^2$ and $\sigma_{\rm I,sp}^2$ are small. The second section is from $w = -1$ to $w = -0.5$, where $\sigma_{\rm I,pl}^2$ and $\sigma_{\rm I,sp}^2$ decrease parabolically. The third section is from $w = -0.5$ to $w = 0$, where $\sigma_{\rm I,pl}^2$ and $\sigma_{\rm I,sp}^2$ increase sharply with the increase of w. Since $-5 < w < -1$ and $-1 < w < 0$ are dominated by temperature fluctuations and salinity fluctuations, respectively, from these curves, we may conclude that salinity fluctuations have greater impact than temperature fluctuations on oceanic turbulence. However, their influences on $\sigma_{\rm I,pl}^2$ and $\sigma_{\rm I,sp}^2$ are not trivial particularly in the second section. In addition, increasing D will reduce $\sigma_{\rm I,pl}^2$

and $\sigma^2_{\mathrm{I,sp}}$, which is more noticeable when the salinity fluctuations dominate the underwater turbulence ($-1 < w < 0$). On the other hand, $\sigma^2_{\mathrm{I,pl}}$ and $\sigma^2_{\mathrm{I,sp}}$ with $d_{\mathrm{r}} = 1$ show different trends, namely, they monotonically increase as w increases from -5 to 0, though from these two curves, it also seems that salinity fluctuations have greater impact than temperature fluctuations on oceanic turbulence. At a fixed receive aperture diameter, Nikishov's spectrum underestimates turbulence strength than Yue's spectrum with $-1 < w < 0$, while it overestimates turbulence strength with $-5 < w < -1$.[15] In both the cases, SI of plane wave is larger than that of spherical wave indicating that spherical wave is less affected by oceanic turbulence.

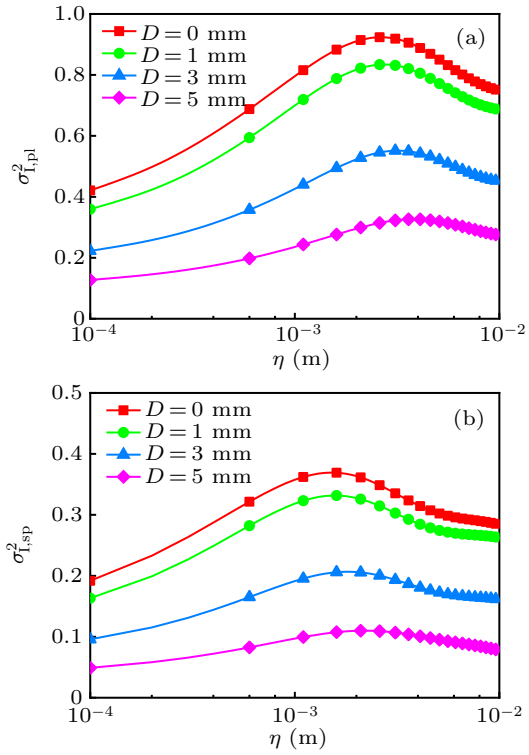


Fig. 2. SI of plane wave (a) and spherical wave (b) versus Kolmogorov microscale length for various receive aperture diameters. For all the curves, $L = 20$ m and $w = -1$.

Next, we show $\sigma^2_{\mathrm{I,pl}}$ and $\sigma^2_{\mathrm{I,sp}}$ as a function of η at certain D in Fig. 2. For each D, $\sigma^2_{\mathrm{I,pl}}$ and $\sigma^2_{\mathrm{I,sp}}$ first increase and then decrease with increasing η, and finally saturate at a level commonly described as the saturation regime.[5,13] The peak values of $\sigma^2_{\mathrm{I,pl}}$ and $\sigma^2_{\mathrm{I,sp}}$ should occur when the random focusing due to large-scale inhomogeneities achieves its strongest effect.[13,14] Then such a focusing effect reduces due to multiple scattering as η further increases. When η is fixed, lower $\sigma^2_{\mathrm{I,pl}}$ and $\sigma^2_{\mathrm{I,sp}}$ are observed for larger D. Such a trend is most obvious when $\sigma^2_{\mathrm{I,pl}}$ and $\sigma^2_{\mathrm{I,sp}}$ are around their peak values. Plane wave is quite sensitive to the η, leading to a higher value of $\sigma^2_{\mathrm{I,pl}}$ than the corresponding $\sigma^2_{\mathrm{I,sp}}$. This is consistent with the case of atmosphere turbulence.[6]

Figure 3 presents SI of plane and spherical wave through oceanic turbulence with respect to L for various D. It can be seen that for each D, $\sigma^2_{\mathrm{I,pl}}$ and $\sigma^2_{\mathrm{I,sp}}$ increase quadratically with increasing L, indicating that UOC system works well only in short to medium distance. There is a significant drop in $\sigma^2_{\mathrm{I,pl}}$ and $\sigma^2_{\mathrm{I,sp}}$ when D increases from 0 mm to 5 mm due to the effect of aperture averaging, especially in long propagation distance, because an increase in L causes a decrease in the receiver intensity correlation and thus the receiver aperture successfully averages all the intensity fluctuations. Given the same L and D, $\sigma^2_{\mathrm{I,pl}}$ is larger than $\sigma^2_{\mathrm{I,sp}}$, which means spherical wave is less affected by oceanic turbulence than plane wave. Particularly, $\sigma^2_{\mathrm{I,pl}}$ with point receiver is about 2.5 times $\sigma^2_{\mathrm{I,sp}}$. The result is similar to that in atmosphere turbulence.[6]

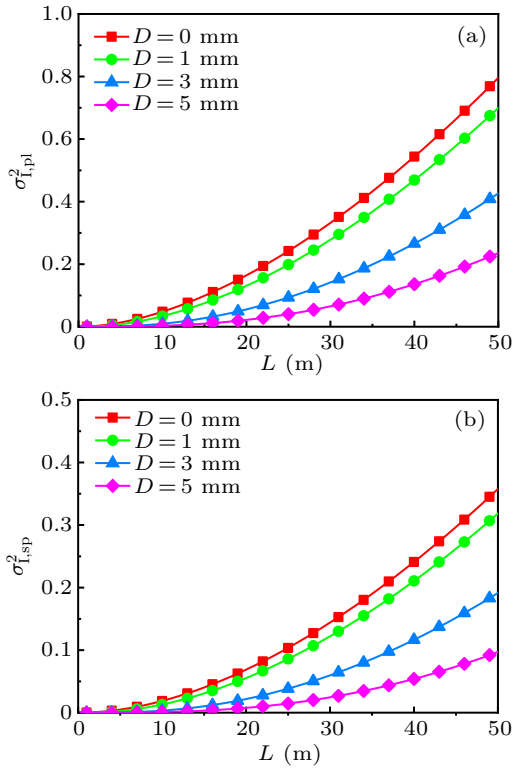


Fig. 3. SI of plane wave (a) and spherical wave (b) versus propagation distance for various receive aperture diameters. For all curves, $w = -1$ and $\eta = 10^{-3}$ m.

In order to demonstrate the validity of our analytic method, SI of plane wave with $D = 0$ mm at different propagation distances is simulated by Monte Carlo simulation,[5] as shown in Fig. 4 (spherical wave is difficult to simulate by Monte Carlo because its infinite beam width). Table 1 gives a comparison between the SI's extracted from the analytic method and the Monte Carlo method. The relative error between the them is less than 10%, proving the rationality of our analytic method.

Next, performance of the UOC system is evaluated for different aperture diameters by investigating typical fade statistics including $Pr(I \le I_{\mathrm{T}})$, $\langle n(I_{\mathrm{T}})\rangle$ and $\langle t(I_{\mathrm{T}})\rangle$ as functions of F_{T} for various D based on the SI. We choose $\upsilon_0 = 550$ Hz in our analysis for the convenience of making comparison between different conditions.[13,16,17]

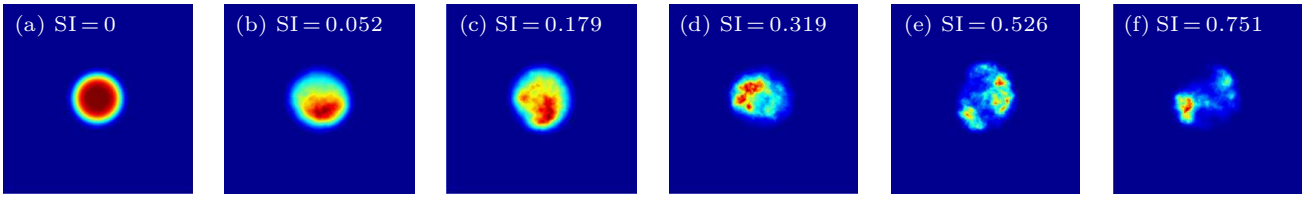


Fig. 4. Plane wave at 0 m (a), 10 m (b), 20 m (c), 30 m (d), 40 m (e) and 50 m (f).

Table 1. SI of plane wave at different propagation distances (SI_1 is from this paper and SI_2 is calculated by the Monte Carlo method).

L (m)	10	20	30	40	50
SI_1	0.048	0.164	0.332	0.544	0.795
SI_2	0.052	0.179	0.319	0.526	0.751
Relative error	8.33%	9.15%	3.92%	3.31%	5.53%

As shown in Fig. 5, $Pr(I \leq I_T)$ decreases with increasing F_T and D. Particularly, increasing F_T by several dB can substantially reduce $Pr(I \leq I_T)$ by several orders of magnitude, especially with large D.[18] $Pr(I \leq I_T)$ of spherical wave is lower than that of plane wave under the same F_T and D. To achieve the same $Pr(I \leq I_T)$ of 10^{-6} under the same D, F_T for spherical wave is again lower than the plane wave. These results indicate that spherical wave is better than the plane wave for UOC.

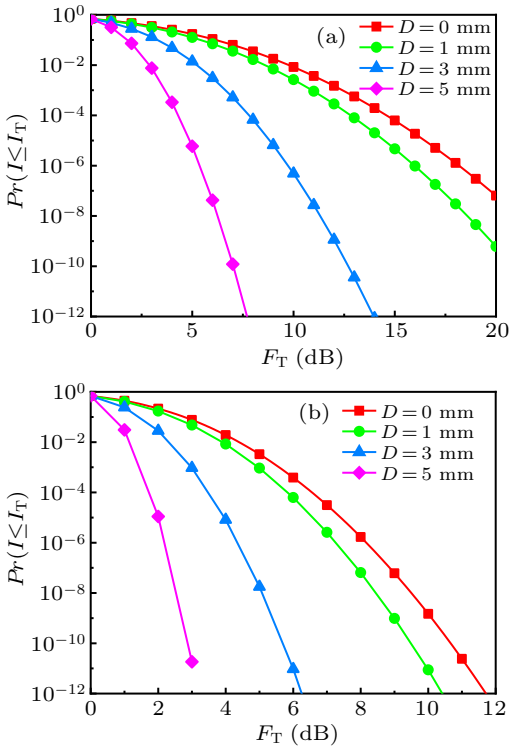


Fig. 5. Probability of fade of plane wave (a) and spherical wave (b) versus F_T for various receive aperture diameters. For all the curves, $L = 20$ m, $w = -1$ and $\eta = 10^{-3}$ m.

Next, the effect of receiving aperture diameter on $\langle n(I_T)\rangle$ for plane and spherical wave is shown in Fig. 6. It can be seen that $\langle n(I_T)\rangle$ firstly reaches the peak value with increasing F_T, then rapidly decreases to low level; and $\langle n(I_T)\rangle$ of the point receiver is the smallest when F_T is set to less than 1dB. On the contrary, if an F_T of more than 1dB is chosen, $\langle n(I_T)\rangle$ decreases with increasing D. To achieve the same $\langle n(I_T)\rangle$, the required F_T value decreases with an increase in D, consistent with the previous studies.[19–22] For example, to achieve the $\langle n(I_T)\rangle$ of 100, F_T of 4.3, 6.1, 8.1 and 9 dB are required for $D = 0$, 1, 3 and 5 mm for plane wave, respectively, where it reduces to 2.8, 4, 5.1 and 5.5 dB, for $D = 0$, 1, 3 and 5 mm for spherical wave, respectively. This means that under the same oceanic turbulence and system parameters, the UOC system with spherical wave has the lower requirement for F_T than that with plane wave. These results also indicate that spherical wave is better than the plane wave for UOC.

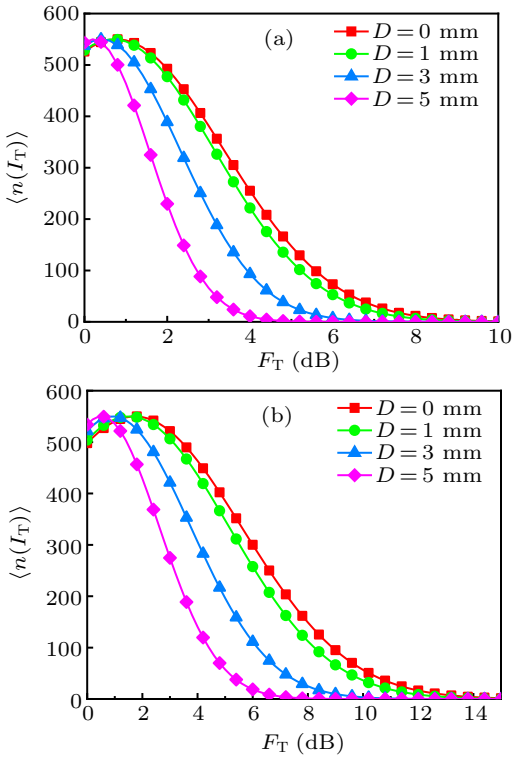


Fig. 6. Expected number of fades versus F_T of plane wave (a) and spherical wave (b) for various receive aperture diameters. For all curves, $L = 20$ m, $w = -1$ and $\eta = 10^{-3}$ m.

Finally, we plot $\langle t(I_T)\rangle$ against F_T with various D in Fig. 7. We can see that $\langle t(I_T)\rangle$ monotonically decreases with F_T. For D less than 1 mm, increasing F_T has no significant impact on $\langle t(I_T)\rangle$. However, when D is larger than 3 mm, $\langle t(I_T)\rangle$ reduces several orders of magnitude by increasing F_T. To achieve a targeted $\langle t(I_T)\rangle$ of 10^{-6} s, the F_T values of 4.3 and 6.9 dB are required for $D = 0$ and 1 mm in the case of

plane wave, respectively, while they reduce to 1.7 and 3.4 dB, respectively, for $D = 0$ and 1 mm in the case of spherical wave. If we want to achieve an acceptable $\langle t(I_T)\rangle$ (for example, 10^{-6} s)[23,24] at $F_T = 5$ dB, D must be larger than 5 mm and 3 mm for plane wave and spherical wave, respectively. This means that spherical wave for UOC can achieve the same $\langle t(I_T)\rangle$ with less difficulty and lower cost than plane wave. These results again indicate that spherical wave is better than the plane wave for UOC.

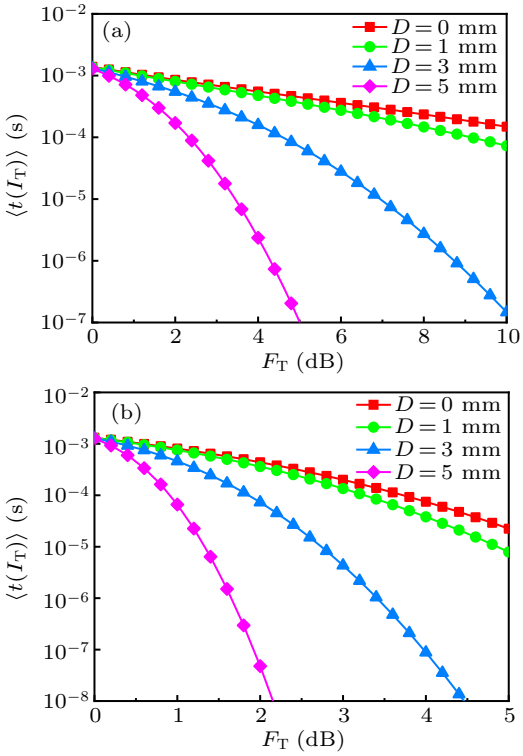


Fig. 7. Mean fade time versus of plane wave (a) and spherical wave for various receive aperture diameters. For all the curves, $L = 20$ m, $w = -1$ and $\eta = 10^{-3}$ m.

In Fig. 8, we plot the SNR in dB as a function of L for various D. SNR_0 is set as 10 dB[25] in our analysis for convenience of making comparison between different conditions. Unsurprisingly, turbulence causes a drop in SNR.[7,8] Particularly, SNR decreases with increasing L and decreasing D. Under the same oceanic condition, the SNR of spherical wave is only slightly better than that of plane wave.

Finally, numerical calculation of the BER against the L for various D leads to the results shown in Fig. 9. These results indicate that to achieve an acceptable level of BER (typically around 10^{-6})[7,8,26] with a receive diameter of 5 mm in the presence of oceanic turbulence, L is required to be limited in 40 m for spherical wave, while it reduces to 15 m for plane wave. This means that under the same BER, spherical wave for UOC can work in longer distance than plane wave, indicating that spherical wave is better than the plane wave for UOC.

It is concluded that the performance of UOC with spherical wave is superior to that of plane wave due to the fact that lower SI leads to lower fade statistics.[27,28] We believe that our results provide a guidance for future UOC systems to choose best parameters such as propagation distance, receiving aperture diameter and fade threshold parameter to fit different ocean conditions.

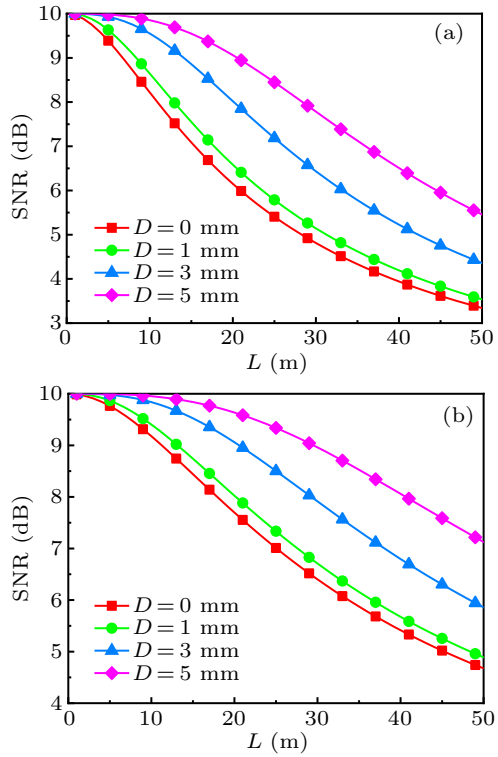


Fig. 8. SNR of plane wave (a) and spherical wave (b) versus propagation distance for various receive aperture diameters. For all the curves, $w = -1$ and $\eta = 10^{-3}$ m.

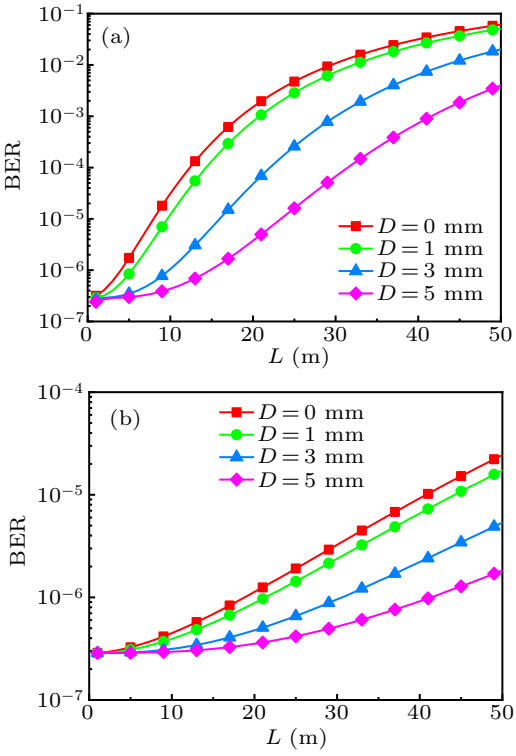


Fig. 9. BER of plane wave (a) and spherical wave (b) versus propagation distance for various receive aperture diameters. For all the curves, $w = -1$ and $\eta = 10^{-3}$ m.

4. Conclusion and perspectives

In summary, we have adopted a spatial power spectrum model that considers the eddy diffusivity ratio and outer scale of turbulence and derived the analytical expressions of SI for plane and spherical waves based on the Rytov theory in weak turbulence. The numerical results show that w, η, L and D play an importance role in SI, while L_0 does not. In many cases, SI based on our model is very different from that based on Nikishov's spectrum. Based on SI, the typical fade statistics of the UOC system including the $Pr(I \le I_{\rm T})$, $\langle n(I_{\rm T})\rangle$, $\langle t(I_{\rm T})\rangle$, SNR and BER are discussed, clearly showing that the UOC system with spherical wave has advantage over that with plane wave. These results are helpful for design of UOC systems in future.

Acknowledgement

We would like to thank Professor Xiang Yi (Xidian University) and Professor Haiping Mei (Anhui Institute of Optics and Fine Mechanics) for helpful discussion and valuable suggestions.

Appendix A

Here, we would show how to calculate $\sigma^2_{\rm I,pl}$ and $\sigma^2_{\rm I,sp}$ in details based on Yue's spectrum. The results are valid for weak oceanic turbulence where SI is below 1.

SI of plane wave is expressed as[13]

$$\sigma^2_{\rm I,pl}(L) = 8\pi^2 k^2 L \int_0^1 \int_0^\infty \kappa \Phi_{\rm n}(\kappa) \exp\left(-\frac{D^2\kappa^2}{16}\right)\left[1-\cos\left(\frac{L\kappa^2}{k}\xi\right)\right] {\rm d}\kappa {\rm d}\xi, \tag{A1}$$

Substituting Eq. (1) into Eq. (A1), $\sigma^2_{\rm I,pl}$ can be expressed as

$$\sigma^2_{\rm I,pl} = 2\pi k^2 L \alpha^2 C_0 \chi_{\rm T} \varepsilon^{-1/3}\left(I_{\rm T,pl} + \frac{d_{\rm r}}{w^2} I_{\rm S,pl} - \frac{1+d_{\rm r}}{w} I_{\rm TS,pl}\right), \tag{A2}$$

with

$$\begin{aligned} I_{\rm i,pl} = {\rm Re}\int_0^1 {\rm d}\xi \int_0^\infty &\left\{\kappa \frac{\exp\left[-\kappa^2/\kappa_{1i}^2\right]}{\left(\kappa^2+\kappa_0^2\right)^{11/6}} - \kappa \frac{\exp\left[-\kappa^2/\kappa_{2i}^2\right]}{\left(\kappa^2+\kappa_0^2\right)^{11/6}}\right\}{\rm d}\kappa \\ &+ {\rm Re} C_i \eta^{2/3} \int_0^1 {\rm d}\xi \int_0^\infty \left\{\kappa^{5/3} \frac{\exp\left[-\kappa^2/\kappa_{1i}^2\right]}{\left(\kappa^2+\kappa_0^2\right)^{11/6}} - \kappa^{5/3} \frac{\exp\left[-\kappa^2/\kappa_{2i}^2\right]}{\left(\kappa^2+\kappa_0^2\right)^{11/6}}\right\}{\rm d}\kappa, \end{aligned} \tag{A3}$$

where $\kappa_{1i}^2 = 1/(\eta^2/N_i^2 + D^2/16)$, $\kappa_{2i}^2 = 1/(\eta^2/N_i^2 + D^2/16 + jL\xi/k)$, j is imaginary number given by $j=(-1)^{1/2}$; ${\rm Re}(x)$ denotes the real part of x.

Using the integral formula in Ref. [12] yields

$$\int_0^\infty \kappa^{2\mu} \frac{\exp\left(-\kappa^2/\kappa_m^2\right)}{\left(\kappa^2+\kappa_0^2\right)^{-11/6}} d\kappa = \frac{1}{2}\kappa_0^{2\mu-8/3}\Gamma\left(\mu+\frac{1}{2}\right) U\left(\mu+\frac{1}{2};\mu-\frac{1}{3};\frac{\kappa_0^2}{\kappa_m^2}\right), \tag{A}$$

where $\Gamma(\cdots)$ represents the gamma function and $U(\cdots)$ represents the confluent hypergeometric function of the second kind.

By performing the integral over κ in Eq. (A3), we obtain

$$\begin{aligned} I_{\rm i,pl} = {\rm Re}\int_0^1 &\frac{1}{2}\kappa_0^{-5/3}\Gamma(1)\left[U\left(1;\frac{1}{6};\frac{\kappa_0^2}{\kappa_{1i}^2}\right) - U\left(1;\frac{1}{6};\frac{\kappa_0^2}{\kappa_{2i}^2}\right)\right]{\rm d}\xi \\ &+ {\rm Re} C_i \eta^{2/3}\int_0^1 \frac{1}{2}\kappa_0^{-1}\Gamma\left(\frac{4}{3}\right)\left[U\left(\frac{4}{3};\frac{1}{2};\frac{\kappa_0^2}{\kappa_{1i}^2}\right) - U\left(\frac{4}{3};\frac{1}{2};\frac{\kappa_0^2}{\kappa_{2i}^2}\right)\right]{\rm d}\xi. \end{aligned} \tag{A5}$$

With the approximation relationship of $U(a;c;z)$ under the condition of $\kappa_0^2/\kappa_{1i}^2 \ll 1$ and $\kappa_0^2/\kappa_{2i}^2 \ll 1$, Eq. (A5) can be further simplified[12] to

$$U(a;c;z) \approx \frac{\Gamma(1-c)}{\Gamma(1+a-c)} + \frac{\Gamma(c-1)}{\Gamma(a)} z^{1-c}, \quad |z| \ll 1. \tag{A6}$$

$$I_{\rm i,pl} = {\rm Re}\int_0^1 \frac{1}{2}\kappa_0^{-5/3}\Gamma\left(-\frac{5}{6}\right)\left[\left(\frac{\kappa_0^2}{\kappa_{1i}^2}\right)^{5/6} - \left(\frac{\kappa_0^2}{\kappa_{2i}^2}\right)^{5/6}\right]{\rm d}\xi + {\rm Re} C_i \eta^{2/3}\int_0^1 \frac{1}{2}\kappa_0^{-1}\Gamma\left(-\frac{1}{2}\right)\left[\left(\frac{\kappa_0^2}{\kappa_{1i}^2}\right)^{1/2} - \left(\frac{\kappa_0^2}{\kappa_{2i}^2}\right)^{1/2}\right]{\rm d}\xi. \tag{A7}$$

Then, by performing the integral over ξ in Eq. (A7), we obtain

$$I_{\rm i,pl} = \frac{1}{2}\Gamma\left(-\frac{5}{6}\right)\left(\frac{\eta^2}{N_i^2}+\frac{D^2}{16}\right)^{5/6}\left\{1 - \frac{6}{11}\left(\frac{16N_i^2 L}{16k\eta^2 + kN_i^2 D^2}\right)^{5/6}\right.$$

$$\times\left[1+\left(\frac{16k\eta^2+kN_i^2D^2}{16N_i^2L}\right)^2\right]^{11/12}\sin\left[\frac{11}{6}\arctan\left(\frac{16N_i^2L}{16k\eta^2+kN_i^2D^2}\right)\right]\Bigg\}$$
$$+\frac{1}{2}C_i\eta^{2/3}\Gamma\left(-\frac{1}{2}\right)\left(\frac{\eta^2}{N_i^2}+\frac{D^2}{16}\right)^{1/2}\left\{1-\frac{2}{3}\left(\frac{16N_i^2L}{16k\eta^2+kN_i^2D^2}\right)^{1/2}\right.$$
$$\left.\times\left[1+\left(\frac{16k\eta^2+kN_i^2D^2}{16N_i^2L}\right)^2\right]^{3/4}\sin\left[\frac{3}{2}\arctan\left(\frac{16N_i^2L}{16k\eta^2+kN_i^2D^2}\right)\right]\right\}. \tag{A8}$$

Here, $\sigma_{\mathrm{I,sp}}^2$, similar to the definition of that of plane wave, is expressed as

$$\sigma_{\mathrm{I,sp}}^2(L)=8\pi^2k^2L\int_0^1\int_0^\infty\kappa\Phi_{\mathrm{n}}(\kappa)\exp\left(-\frac{D^2\kappa^2\xi^2}{16}\right)\left\{1-\cos\left[\frac{L\kappa^2}{k}\xi(1-\xi)\right]\right\}\mathrm{d}\kappa\mathrm{d}\xi. \tag{A9}$$

Similar to the plane wave, $\sigma_{\mathrm{I,sp}}^2$ can be expressed as

$$\sigma_{\mathrm{I,sp}}^2=2\pi k^2L\alpha^2C_0\chi_{\mathrm{T}}\varepsilon^{-1/3}\left(I_{\mathrm{T,sp}}+\frac{d_{\mathrm{r}}}{w^2}I_{\mathrm{S,sp}}-\frac{1+d_{\mathrm{r}}}{w}I_{\mathrm{TS,sp}}\right), \tag{A10}$$

with

$$I_{\mathrm{i,sp}}=\mathrm{Re}\int_0^1\mathrm{d}\xi\int_0^\infty\left\{\kappa\frac{\exp\left[-\kappa^2/\kappa_{1i}^2\right]}{\left(\kappa^2+\kappa_0^2\right)^{11/6}}-\kappa\frac{\exp\left[-\kappa^2/\kappa_{2i}^2\right]}{\left(\kappa^2+\kappa_0^2\right)^{11/6}}\right\}\mathrm{d}\kappa$$
$$+\mathrm{Re}C_i\eta^{2/3}\int_0^1\mathrm{d}\xi\int_0^\infty\left\{\kappa^{5/3}\frac{\exp\left[-\kappa^2/\kappa_{1i}^2\right]}{\left(\kappa^2+\kappa_0^2\right)^{11/6}}-\kappa^{5/3}\frac{\exp\left[-\kappa^2/\kappa_{2i}^2\right]}{\left(\kappa^2+\kappa_0^2\right)^{11/6}}\right\}\mathrm{d}\kappa, \tag{A11}$$

where $\kappa_{1i}^2=1/(\eta^2/N_i^2+D^2/16)$, $\kappa_{2i}^2=1/[\eta^2/N_i^2+D^2/16+jL\xi(1-\xi)/k]$.

Utilizing similar processing methods to plane wave, $I_{\mathrm{i,sp}}$ can be derived as

$$I_{\mathrm{i,sp}}=\frac{1}{2}\Gamma\left(-\frac{5}{6}\right)\left(\frac{\eta}{N_i}\right)^{5/3}\frac{144\eta^2}{11N_i^2D^2}\left[\left(1+\frac{N_i^2D^2}{24\eta^2}\right)^{11/6}-1\right]$$
$$-\frac{1}{2}\Gamma\left(-\frac{5}{6}\right)\left(\frac{\eta}{N_i}\right)^{5/3}\mathrm{Re}\left[{}_2F_1\left(-5/6,1;2;-\frac{jLN_i^2}{k\eta^2}+\frac{2}{3}\left(j\frac{kD^2}{16L}+1\right)\frac{jLN_i^2}{k\eta^2}\right)\right]$$
$$+\frac{1}{2}C_i\eta^{2/3}\Gamma\left(-\frac{1}{2}\right)\left(\frac{\eta}{N_i}\right)\frac{16\eta^2}{N_i^2D^2}\left[\left(1+\frac{N_i^2D^2}{24\eta^2}\right)^{3/2}-1\right]$$
$$-\frac{1}{2}C_i\eta^{2/3}\Gamma\left(-\frac{1}{2}\right)\left(\frac{\eta}{N_i}\right)\mathrm{Re}\left[{}_2F_1\left(-1/2,1;2;-\frac{jLN_i^2}{k\eta^2}+\frac{2}{3}\left(j\frac{kD^2}{16L}+1\right)\frac{jLN_i^2}{k\eta^2}\right)\right]. \tag{A12}$$

Based on the approximate formula of generalized hypergeometric function ${}_1F_2(1-a,1;2;-x)=\frac{(1+x)^a-1}{ax}$, we can obtain

$$\mathrm{Re}\left[{}_2F_1\left(-5/6,1;2;-\frac{jLN_i^2}{k\eta^2}+\frac{2}{3}\left(j\frac{kD^2}{16L}+1\right)\frac{jLN_i^2}{k\eta^2}\right)\right]=-\frac{\frac{3kD^2}{8L}}{\frac{11}{6}\left(\frac{LN_i^2}{k\eta^2}\right)\left(1+\frac{k^2D^4}{64L^2}\right)}$$
$$+\left(\frac{LN_i^2}{k\eta^2}\right)^{5/6}\frac{\left[1+\left(\frac{kD^2}{8L}+\frac{3k\eta^2}{LN_i^2}\right)^2\right]^{11/12}}{\frac{11}{6}3^{5/6}\left(1+\frac{k^2D^4}{64L^2}\right)^{1/2}}\sin\left[\frac{11}{6}\tan^{-1}\left[\left(\frac{3k\eta^2}{LN_i^2}+\frac{kD^2}{8L}\right)^{-1}\right]+\tan^{-1}\left(\frac{kD^2}{8L}\right)\right], \tag{A13}$$

$$\mathrm{Re}\left[{}_2F_1\left(-1/6,1;2;-\frac{jLN_i^2}{k\eta^2}+\frac{2}{3}\left(j\frac{kD^2}{16L}+1\right)\frac{jLN_i^2}{k\eta^2}\right)\right]=-\frac{\frac{3kD^2}{8L}}{\frac{3}{2}\left(\frac{LN_i^2}{k\eta^2}\right)\left(1+\frac{k^2D^4}{64L^2}\right)}$$
$$+\left(\frac{LN_i^2}{k\eta^2}\right)^{1/2}\frac{\left[1+\left(\frac{kD^2}{8L}+\frac{3k\eta^2}{LN_i^2}\right)^2\right]^{3/4}}{\frac{3}{2}3^{1/2}\left(1+\frac{k^2D^4}{64L^2}\right)^{1/2}}\sin\left[\frac{3}{2}\tan^{-1}\left[\left(\frac{3k\eta^2}{LN_i^2}+\frac{kD^2}{8L}\right)^{-1}\right]+\tan^{-1}\left(\frac{kD^2}{8L}\right)\right]. \tag{A14}$$

References

[1] Hanson F and Radic S 2008 *Appl. Opt.* **47** 277
[2] Johnson L J, Green R J and Leeson M S 2013 *Appl. Opt.* **52** 7867
[3] Chan V W S 2006 *J. Lightwave Technol.* **24** 4750
[4] Nikishov V V and Nikishov V I 2000 *Int. J. Fluid Mech. Res.* **27** 82
[5] Korotkova O, Farwell N and Shchepakina E 2012 *Waves in Random and Complex Media* **22** 260
[6] Wang Z Q, Zhang P F, Qiao C H, Lu L, Fan C Y and Ji X L 2016 *Opt. Commun.* **380** 79
[7] Yi X, Li Z and Liu Z J 2015 *Appl. Opt.* **54** 1273
[8] Yi X, Liu Z J and Yue P 2013 *Opt. Laser Technol.* **47** 199
[9] Gokce M C and Baykal Y 2018 *Opt. Commun.* **410** 830
[10] Baykal Y 2016 *Appl. Opt.* **55** 1228
[11] Elamassie M, Uysal, M, Baykal Y, Abdallah M and Qaraqe K 2017 *Opt. Soc. Am. A* **34** 1969
[12] Yue P, Luan X H, Yi X, Cui Z M and Wu M.J 2019 *Opt. Soc. Am. A* **36** 556
[13] Andrew L C and Phillips R L 2005 *Laser Beam Propagation Through Random Medium* 2nd edn (Washington: SPIE Press) pp. 261–269
[14] Li Y, Zhang Y X and Zhu Y 2018 *Opt. Commun.* **428** 57
[15] Yue P, Wu M J, Yi X, Cui Z M and Luan X H 2018 *Opt. Soc. Am. A* **36** 32
[16] Al-Habash M A, Andrews L C and Phillips R L 2001 *Opt. Eng.* **40** 1554
[17] Chan V W S 2006 *J. Lightwave Technol.* **24** 4750
[18] Yura H T and McKinley W G 1983 *Appl. Opt.* **22** 3353
[19] Andrews L C, Phillips R L and Hopen C Y 2000 *Waves in Random and Complex Media* **10** 53
[20] Luan X H, Yue P and Yi X 2019 *Opt. Soc. Am. A* **36** 2048
[21] Wu T, Ji X L, Li X Q, Wang H, Deng Y and Deng Z L 2018 *Acta Phys. Sin.* **67** 224206 (in Chinese)
[22] Wei Y, Liu F, Yang K, Han P L, Wang X H and Shao X P 2018 *Acta Phys. Sin.* **67** 184202 (in Chinese)
[23] Wu T, Ji X L and Luo Y J 2018 *Acta Phys. Sin.* **67** 054206 (in Chinese)
[24] Wu X Y, Kong M, Li G Y and Zhao W J 2009 *Acta Phys. Sin.* **58** 2654 (in Chinese)
[25] Bi W H, Chen J G and Zhang S 2017 *Acta Phys. Sin.* **66** 074206 (in Chinese)
[26] Zhang X H, Zhang S and Sun C S 2016 *Acta Phys. Sin.* **65** 144204 (in Chinese)
[27] Liu D J, Wang Y C, Wang G Q, Yin H M and Zhong H Y 2019 *Chin. Phys. B* **28** 104207
[28] Guo L X, Wang R and Wu Z S 2010 *Chin. Phys. B* **19** 044102